Available online at www.sciencedirect.com
ScienceDirect
Progress in Natural Science 18 (2008) 707–711
Progress in Natural Science
www.elsevier.com/locate/pnsc

Full-angle optical imaging of near-infrared fluorescent probes implanted in small animals

Gang Hu, Junjie Yao, Jing Bai *

Department of Biomedical Engineering, Tsinghua University, Beijing 100084, China

Received 22 October 2007; received in revised form 27 November 2007; accepted 27 November 2007

Abstract

To provide a valuable experimental platform for *in vivo* biomedical research of small animal model with fluorescence mediated approach, we developed a whole-body near-infrared fluorescence molecular imaging system as described in this paper. This system is based on a sensitive CCD camera and has the ability to achieve 360° full-angle source illuminations and projections capture of the targets to obtain the dense sampling by performing rotational scan. The measurement accuracy is validated from cylinder phantom experiments by the comparison between the experimental data and theoretical predictions. Finally, we also present typical *in vivo* images of fluorescent tube implanted into the mouse body. The results are promising and have proved the system imaging performance for macroscopic optical biomedical research.

Keywords: Fluorescence molecular imaging; Small animal imaging; Fluorescent probe

1. Introduction

As a newly emerged optical imaging method, fluorescence molecular imaging (FMI) technique has received increasing attention due to its ability of non-invasive visualization of the molecular and cellular activities in living subjects [1]. These advantages benefit bioengineering scientists to investigate disease process, evaluate therapy, respond and develop new drugs [2]. In comparison with other molecular imaging approach, fluorescence molecular imaging can realize a high sensitivity detection with low instrumentation expense, furthermore, the fast imaging speed facilitates the high-throughput study of biological processes in animal tissue. The whole-body small animal fluorescence imaging commonly suffers from the inherent characteristic of high tissue absorption to the low-energy photon, which results in fluorescence images with low signal-to-background contrast. This problem has been partly solved by the utilization of near-infrared (NIR) fluorochromes with absorption and emission spectrum located at 650–900 nm. Imaging in this wavelength region can obtain maximum several centimeters detection depth [3,4]. The emergence of sensitive, cooled, charged coupled device (CCD) also facilitates the parallel detection of multi-channel fluorescent signals at low intensity levels.

Several new CCD-based fluorescence imaging systems have employed planar geometry detection setup beyond the traditional cylinder scheme [5–8]. In these systems, the CCD camera directly captures photons emitted from transparent optical chamber to obtain the dense spatial sampling, which is useful to reconstruct high resolution tomography images. The emergence of non-contact technique allows photon detection without the need of matching liquid surrounding animals, which can decrease the unwanted fluorescence intensity attenuation as well as significantly simplifying the experimental procedure [9,10]. But the planar imaging systems have their inherent limit

* Corresponding author. Tel.: +86 10 62786480; fax: +86 10 62786480.
E-mail address: deabj@tsinghua.edu.cn (J. Bai).

1002-0071/$ - see front matter © 2007 National Natural Science Foundation of China and Chinese Academy of Sciences. Published by Elsevier Limited and Science in China Press. All rights reserved.
doi:10.1016/j.pnsc.2007.11.021

in a fixed area to illuminate the target and also in a fixed small view angle to monitor the fluorescent signals [11,12]. So we attempted to develop a prototype experimental platform that permits complete-angle illumination and projections scan view of small animals. This implementation should have the ability of obtaining fluorescence images from any direction to provide full-view dataset for high-quality 3D map reconstruction of inner fluorochrome.

In this paper, we describe the detailed hardware setup first and then the tissue phantom experiments performed for the evaluation of the measurement performance. Finally, the preliminary results from *in vivo* phantom test are presented.

2. Instrumentation design

The hardware system used to record diffuse optical signals has a similar setup to X-ray computed tomography. The configuration is shown in Fig. 1.

A continuous-wave laser operating at 671 nm wavelength launches lights of 200 mW max output power. The laser beam is coupled to a lens to focus on the one side boundary of target with the spot diameter less than 1 mm. The signal collection of transmitted photons is finished by a cooled electron multiplying CCD (EMCCD) camera placed on the opposite side. The CCD chip can be cooled down to −85 °C to reduce the dark current noise. The camera has an active pixel array of 512 × 512 and 14-bit available digitization. The quantum efficiency for 650–900 nm light is above 80% for high-sensitive detection of weak fluorescent signals. A 60 mm imaging lens allows an approximate view field of 2.5 × 2.5 cm at the closest focusing distance of about 20 cm. Fluorescent images are captured by placing a bandpass filter with center wavelength of 705 nm, FWHM of 10 nm in front of the camera lens. The attenuation of the fluorescent filter for intrinsic light is at the level of 10^{-5}. The target (tissue phantom or small animal) is fixed with a replaceable holder which is equipped on a rotation stage with a resolution of 0.0025°, repeatability error less than 0.01°. The rotation parameters such as speed and direction can be set by the motor controller. All operations of mechanical rotation and image capture are controlled by a personal computer.

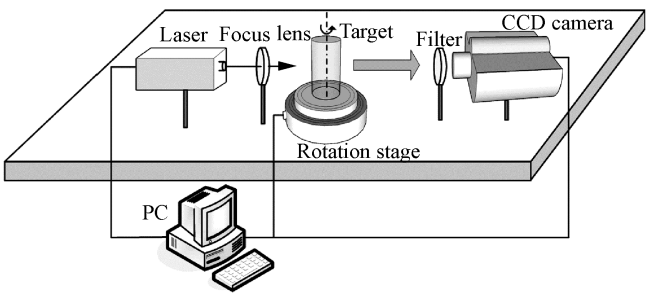

Fig. 1. Experimental setup of full-angle fluorescence imaging system. Only tissue phantom is presented in this figure. The small animal can be fixed on the rotation stage by a home-made holder.

3. Comparison between experimental data and theoretical prediction

We ought to examine the validation of the dataset collected by this imaging system. The test can be made by the comparison between the experimental results and the theoretical prediction. A feasible approach is to evaluate the photon field images from a tissue phantom with known geometry and optical properties. The phantom used here is made of an intralipid-ink mixture solution with absorption coefficient of 0.25 cm^{-1} and reduced scattering coefficient of 15 cm^{-1}. The solution is infused into a glass cylinder with a height of 70 mm and an inner diameter of 25 mm. The container is then fixed on the rotation stage and positioned at the middle view field of the camera. The laser beam shines on the center axis of the container side and the focus point is 20 mm away from the top edge. In this experiment, we did not insert any probe into the solution to create fluorescent signals. It is feasible to utilize the detected diffuse signals to check the data validation because the diffuse lights at the excitation wavelength and fluorescence at the emission wavelength has trivial difference in propagation model. Furthermore, the excitation light generally has better signal quality than fluorescence, which is more suitable for accuracy estimation. In this experiment, the expose time for excitation images capture was set less than 100 ms without pixel saturation. The region for analysis was selected as a rectangle region of 20 × 8 mm, corresponding to 21 × 9 measurements (see Fig. 2). Each measurement value came from an average intensity of 4 × 4 adjacent pixels.

The distribution of diffuse photon field can be predicted by diffusion approximation equation with boundary condition restrict [12]. The Green's function has provided an analytical forward solution to homogeneous object with simple geometry as used in our experiments. Actually we can calculate the theoretical optical intensity at the cylinder surface with a code from the site (http://esperia.iesl.forth.gr/~jripoll/). The optical intensity J at phantom surface S can be related to the measurements P at the CCD with a free-space propagation equation [13]:

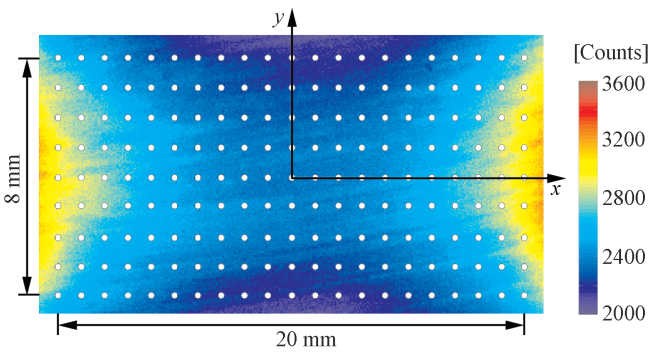

Fig. 2. The diagram of the region selected for the data agreement evaluation. The circles over the excitation images denote the position of 21 × 9 measurements.

$$P(r_d) = \frac{1}{\pi}\int_S J(r)T(r,r_d)\mathrm{d}S \quad r \in S \tag{1}$$

where T mainly expresses the relative positions of the imaging region to the virtual detector array in the CCD chip.

The comparison between the values predicted by forward simulation model and the measurements from cylinder phantom is shown in Fig. 3. The selected region covers the center quarter area in the field of view. The experimental curve (triangle) is plotted by data on the phantom surface by use of the inversion of Eq. (1). All data have been normalized to their maximum intensity. Good agreement (errors less than 5%) can be obtained particularly in the center region due to its location well in focal plane of the CCD camera. The difference may come from the measurement noise, propagation model approximation and phantom parameter tolerance.

4. Phantom fluorescent imaging

We also performed experiments of imaging on a target embedded in diffuse media to examine the system's detection ability of fluorescent signals. The target was made of a glass capillary called as a fluorescent tube with an inner diameter of 0.7 mm and a length of 6 mm. The Cy5.5 dye at concentration of 2 μM was injected into the tube. The Cy5.5 dye has absorption peak at 678 nm and emission peak at 704 nm. The sealed tube was inserted into the cylinder container and located 10 mm away from the rotation axis as shown in Fig. 4. The diffuse solution has the same recipe to the above excitation light experiments. In Fig. 5, we show images at four typical angular positions. The 0° and 180° images are corresponding to the fluorescent tube situated with a depth of 2.5 mm and 22.5 mm away from the focal plane, respectively. The size of the images is 200 × 200 pixel over 12 × 12 mm square region. It can be seen that the highly scattering property would blur the images. So, the imaging performance depends on the relative position of the target to the light source and the detector. The fluorescent target's concentration and position can be resolved by optical tomography technique [14].

We checked the reproducibility of this imaging system by comparison of fluorescence imaging at the angular positions of 0° and 360°. Five measurement cycles were made in this test. The averaged 0° image was divided by averaged 360° image pixel by pixel to create a normalized image with a size of 200 × 200 pixel. The normalized data showed a normal density distribution with stable mean value of about 1.002 and standard deviation less than 0.004.

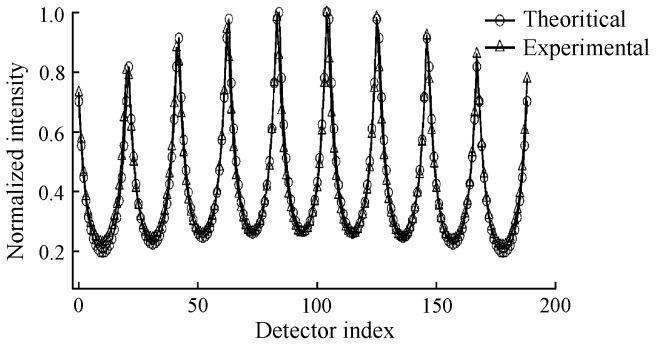

Fig. 3. Evaluation of the agreement between the predictions and experimental data. All values are scaled to the maximum intensity.

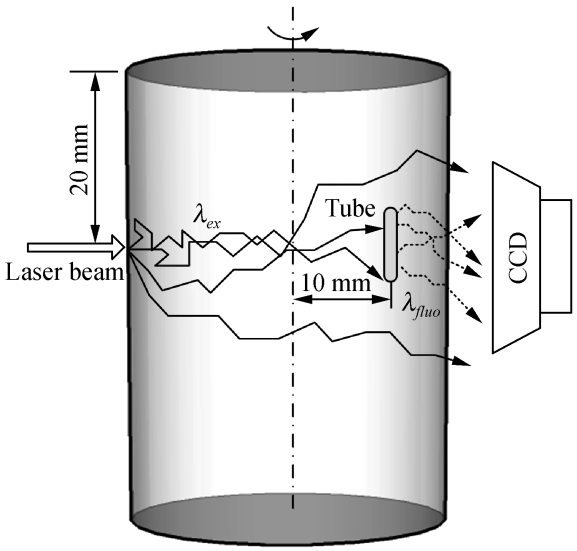

Fig. 4. Side view of the experimental setup for fluorescence measurements. The fluorescent tube is placed at the initial 0° position with 10 mm distance to the axis.

We also searched the two maximum intensity positions in the 0° and 360° images by the use of an appropriate threshold and weighted function and found that the distance between the two positions was less than 0.2 mm. The reproducibility errors were mainly caused by mechanical instabilities of the rotation. However, this accuracy was qualified for whole-body diffuse optical imaging.

5. Small animal imaging

Our ultimate goal is to perform fluorescent imaging of small animals. Imaging the living animals can bring more problems than in phantom experiments. We have found that the irregular shape of animals complexed the adjustment of view field especially in rotation status. The heterogeneity of the animals may decrease the image quality because some regions with high vascular distribution such as liver and spleen can severely attenuate optical signals, which results in less fluorescent photons arriving at detectors. Moreover, the autofluorescence caused by skin collagen and elastins may deteriorate the image contrast [15]. Fortunately, the transillumination imaging setup in this system can partly decrease the effect. In our experiments, a four-week-old mouse was chosen as the target. To maximize the photons arriving at the detector, shaving of the mouse fur is necessary. The mouse was anaesthetized and two fluorescent capillaries filled with 8 μM Cy5.5 dye were implanted at different depths (about 3 mm and 5 mm to the abdomen surface) to simulate tumors. White-light images

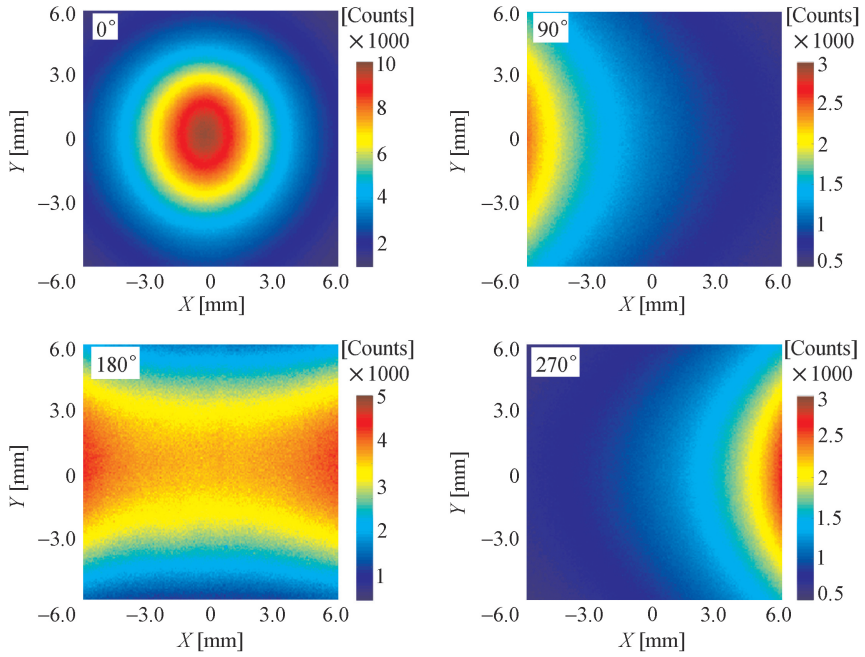

Fig. 5. Phantom fluorescence images captured by CCD from typical positions in a measurement cycle.

without placing any filters and fluorescence images with exposure time of 5 s were captured with 120 projections in a cycle. Fig. 6 shows the results from *in vivo* phantom experiments at two typical angular positions of 0° and 180°. The tube depth at 180° position is larger than 10 mm. Fig. 6(a and d) are the white-light mouse image used as the positional reference for overlays. (b and e) Depict the corresponding fluorescence images in the pseudocolor mode. Merged images are shown in (c and f) for simultaneous visualization after threshold setting for removing low background intensity. The observed signal-to-background ratios of the two fluorochromes are both above 25 dB.

6. Conclusions

In this paper, we report an experimental system that can obtain the 360° projection fluorescent images of tissue phantom or small animals. This feature allows complete visualization of targets to maximize the angular information contents. The non-contact configuration facilitates the experimental procedures and widens its application due to the absence of matching liquid. It is clear that fast images acquisition speed is important for *in vivo* study, so single excitation source ring is used in this system and this is enough for transillumination imaging. If 120 projections are acquired, the total capture time is less than 15 min,

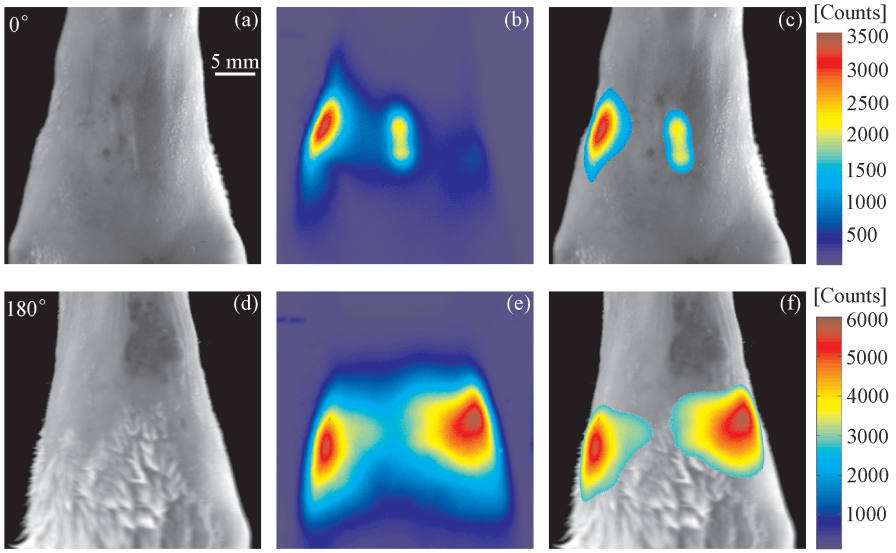

Fig. 6. Living mouse images with two fluorescent capillaries embedded into the body. White-light illumination images are shown in (a and d). (b and e) Are fluorescence images. The merged images (c and f) indicate the relative position of the fluorochrome to the background.

which is about double acquisition efficiency compared to some reported systems [11]. Actually, we have redesigned the stage that can be lifted in vertical direction to implement a multi-ring source scanning. The maximal pixel resolution at the smallest field of view can achieve 50 μm, which is very suitable for detailed observations.

We have obtained good data accuracy proved by comparing the measured values to the theoretical prediction with a phantom model. Results from fluorescence measurements of phantom and animals have demonstrated the system ability of providing high-quality raw dataset for later analysis.

Actually, our ultimate destination is the tomographic visualization of biological events in deep tissues. The results shown in this paper is a preliminary work for the future localization and quantification of fluorescent makers in living animals based on the inversion reconstruction of the fluorescence amplitude. We have found that the measurement performance can be further improved by better optimizing the arrangement of illumination source and view field. Moreover, we are developing now a new light source which can launch excitation signals at a larger spectrum region to satisfy different fluorescent probes. Overall, the system at this moment can serve as a powerful experimental platform for fluorescence molecular imaging study on a living animal.

Acknowledgements

This work was supported by the National Natural Science Foundation of China (Grant Nos. 30670577, 60571013, 60331010), the National Basic Research Program of China (No. 2006CB705700) and the Hi-Tech Research and Development Program of China (No. 2006AA020803).

References

[1] Ntziachristos V, Ripoll J, Wang LHV, et al. Looking and listening to light: the evolution of whole-body photonic imaging. Nat Biotechnol 2005;23:313–20.
[2] Massoud TF, Gambhir SS. Molecular imaging in living subjects: seeing fundamental biological processes in a new light. Genes Dev 2003;17:545–80.
[3] Weissleder R, Ntziachristos V. Shedding light onto live molecular targets. Nat Med 2003;9:123–8.
[4] Ntziachristos V, Ripoll J, Weissleder R. Would near-infrared fluorescence signals propagate through large human organs for clinical studies? Opt Lett 2002;27:333–5.
[5] Graves EE, Ripoll J, Weissleder R, et al. A submillimeter resolution fluorescence molecular imaging system for small animal imaging. Med Phys 2003;30:901–11.
[6] Zacharakis G, Ripoll J, Weissleder R, et al. Fluorescent protein tomography scanner for small animal imaging. IEEE Trans Med Imaging 2005;24:878–85.
[7] Ntziachristos V, Urner G, Dunham J, et al. Planar fluorescence imaging using normalized data. J Biomed Opt 2005;10:064007.
[8] Ntziachristos V, Weissleder R. Charge-coupled-device based scanner for tomography of fluorescent near-infrared probes in turbid media. Med Phys 2002;29:803–9.
[9] Schulz RB, Ripoll J, Ntziachristos V. Noncontact optical tomography of turbid media. Opt Lett 2003;28:1701–3.
[10] Schulz RB, Ripoll J, Ntziachristos V. Experimental fluorescence tomography of tissues with noncontact measurements. IEEE Trans Med Imaging 2004;23:492–500.
[11] Deliolanis N, Lasser T, Hyde D, et al. Free-space fluorescence molecular tomography utilizing 360 degrees geometry projections. Opt Lett 2007;32:382–4.
[12] Meyer H, Garofaiakis A, Zacharakis G, et al. Noncontact optical imaging in mice with full angular coverage and automatic surface extraction. Appl Opt 2007;46:3617–27.
[13] Ripoll J, Schulz RB, Ntziachristos V. Free-space propagation of diffuse light: theory and experiments. Phys Rev Lett 2003;91:103901.
[14] Arridge SR. Optical tomography in medical imaging. Inverse Probl 1999;15:R41–93.
[15] Mansfield JR, Gossage KW, Hoyt CC, et al. Autofluorescence removal, multiplexing, and automated analysis methods for *in-vivo* fluorescence imaging. J Biomed Opt 2005;10:04120.